Offset Between Profiling Float and Shipboard Oxygen Observations at Depth Imparts Bias on Float pH and Derived pCO$_2$

Seth M. Bushinsky[1] , Zachary Nachod[1], Andrea J. Fassbender[2] , Veronica Tamsitt[3] , Yuichiro Takeshita[4] , and Nancy Williams

[1]Department of Oceanography, School of Earth and Space Science and Technology, University of Hawai'i at Mānoa, Honolulu, HI, USA, [2]NOAA/OAR Pacific Marine Environmental Laboratory, Seattle, WA, USA, [3]University of South Florida, St. Petersburg, FL, USA, [4]Monterey Bay Aquarium Research Institute, Moss Landing, CA, USA

Abstract Profiles of oxygen measurements from Argo profiling floats now vastly outnumber shipboard profiles. To correct for drift, float oxygen data are often initially adjusted to deployment casts, ship-based climatologies, or, recently, measurements of atmospheric oxygen for in situ calibration. Air calibration enables accurate measurements in the upper ocean but may not provide similar accuracy at depth. Using a quality controlled shipboard data set, we find that the entire Argo oxygen data set is offset relative to shipboard measurements (float minus ship) at pressures of 1,450–2,000 db by a median of −1.9 µmol kg^{-1} (mean ± SD of −1.9 ± 3.9, 95% confidence interval around the mean of {−2.2, −1.6}) and air-calibrated floats are offset by −2.7 µmol kg^{-1} (−3.0 ± 3.4 (CI$_{95\%}${−3.7, −2.4})). The difference between float and shipboard oxygen is likely due to offsets in the float oxygen data and not oxygen changes at depth or biases in the shipboard data set. In addition to complicating the calculation of long-term ocean oxygen changes, these float oxygen offsets impact the adjustment of float nitrate and pH measurements, therefore biasing important derived quantities such as the partial pressure of CO$_2$ (pCO$_2$) and dissolved inorganic carbon. Correcting floats with air-calibrated oxygen sensors for the float-ship oxygen offsets alters float pH by a median of 3.0 mpH (3.1 ± 3.7) and float-derived surface pCO$_2$ by −3.2 µatm (−3.2 ± 3.9). This adjustment to float pCO$_2$ represents half, or more, of the bias in float-derived pCO$_2$ reported in studies comparing float pCO$_2$ to shipboard pCO$_2$ measurements.

Plain Language Summary Oxygen has historically been measured using chemical titrations on water collected by ships at sea. Over the past 20 years, sensors that measure oxygen have been deployed on robotic profiling floats. Measurements by oxygen sensors on profiling floats greatly exceed those collected by ships. Here, we compare all available float oxygen data to shipboard measurements in deep waters (1,450–2,000 m depth) where we do not expect oxygen to change in the ocean. We find a difference between float and shipboard data. If left uncorrected, this difference would give the false impression of a long-term oxygen change. This difference also impacts float-measured pH and float-estimated carbon dioxide, both of which rely on float oxygen measurements. Correcting oxygen, and therefore float pH and carbon dioxide, would largely address a widely studied bias in float measurements of these parameters.

1. Introduction

Measurements of oxygen in the ocean are critical as the ocean is losing oxygen due to warming, respiration, and stratification-induced changes in ventilation (Helm et al., 2011; Levin, 2018; Schmidtko et al., 2017; Stramma & Schmidtko, 2021). Measurements of ocean oxygen can also be used to understand the balance between photosynthesis and respiration in the surface and deep oceans (Bushinsky & Emerson, 2015; Emerson, 1987; Hennon et al., 2016; Yang et al., 2017). Historically, oxygen was measured primarily by Winkler titrations of water sampled from the ocean (Carpenter, 1965; A. G. Dickson, 1994). These titrations require reliable standards and trained operators to achieve high accuracy and precision. Winkler titrations have been supplemented by electrochemical and optical sensors attached to CTDs but have remained the gold standard of accurate oxygen measurement in the ocean.

Oxygen measurements on autonomous profiling floats are transforming our ability to observe the ocean at unprecedented levels of detail. The first Argo oxygen data was from floats deployed in the early 2000s equipped with Clark-cell electrodes (Figure 1) that provided fast response times but could drift rapidly and in unpredictable

Software: Seth M. Bushinsky,
Zachary Nachod, Veronica Tamsitt,
Yuichiro Takeshita, Nancy Williams
Supervision: Seth M. Bushinsky,
Yuichiro Takeshita, Nancy Williams
Validation: Seth M. Bushinsky
Visualization: Seth M. Bushinsky,
Zachary Nachod
Writing – original draft: Seth
M. Bushinsky
Writing – review & editing: Seth
M. Bushinsky, Zachary Nachod, Andrea
J. Fassbender, Veronica Tamsitt
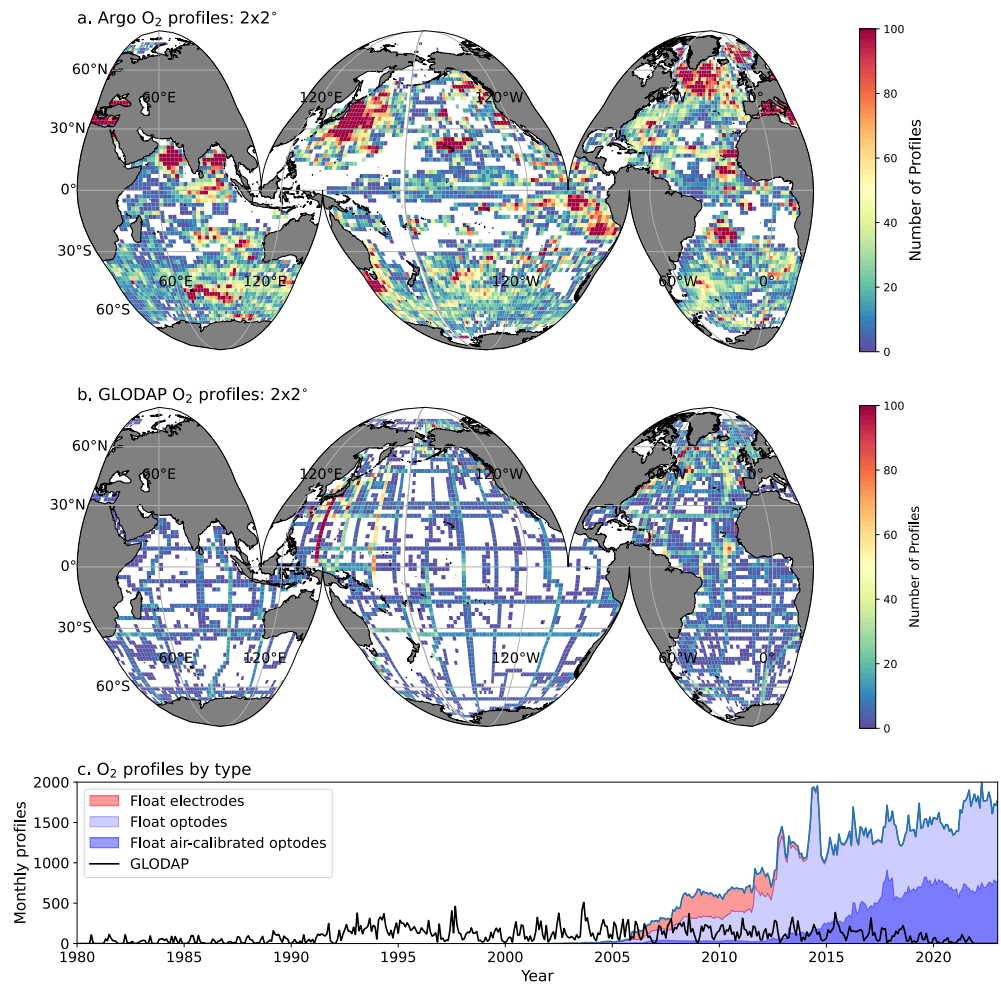
Figure 1. Observational density of float and ship oxygen and change in float sensor type over time. Float (a) and Global Ocean Data Analysis Project (GLODAP) (b) oxygen profile density on a $2 \times 2°$ grid. (c) Total number of oxygen profiles per month, with the contribution of float sensor type shown (Clark cell electrodes (red) and optodes (blue), and the subset of optodes calibrated with in-air measurements (dark blue)), and total number of GLODAP profiles that contain oxygen per month (black line). 2,162 Argo floats deployed between 2002 and 2024 were included in this data set.

ways (Gruber et al., 2007). Oxygen optodes that measure the partial pressure of oxygen through an oxygen-sensitive luminophore have now become the standard oxygen sensor deployed on floats (Claustre et al., 2020; Gruber et al., 2009; Körtzinger et al., 2005; Tengberg et al., 2006) (Figure 1). Over 2100 Argo oxygen floats have been deployed as of 2024, with increasing numbers due to a mix of many small deployments by individual research groups and the development of a few projects deploying large numbers of floats (e.g., the Southern Ocean Carbon and Climate Observations and Modeling project, SOCCOM (Johnson et al., 2017; Sarmiento et al., 2023); Global Ocean Biogeochemistry Array, GO-BGC (Roemmich et al., 2021; Schofield, O. A. et al., 2022)). Optodes drift significantly prior to deployment and corrections to Winkler oxygen measurements from deployment casts or to climatological oxygen have been used in the past (D'Asaro & McNeil, 2013; Drucker & Riser, 2016; Takeshita et al., 2013). The advent of calibration using atmospheric oxygen has since increased the accuracy of surface data to better than 1% (Bittig, Körtzinger, et al., 2018; Bushinsky et al., 2016; Johnson et al., 2015). At the level of accuracy needed for oxygen sensors in the ocean, atmospheric oxygen is essentially constant. Optodes measure oxygen in either air or water; therefore, by measuring the atmospheric partial pressure of oxygen, a reference point can be obtained upon surfacing:

$$p O_2^{atmos} = \left(P_{Atm} - p H_2O \left(\frac{RH}{100} \right) \right) X_{O_2} \tag{1}$$
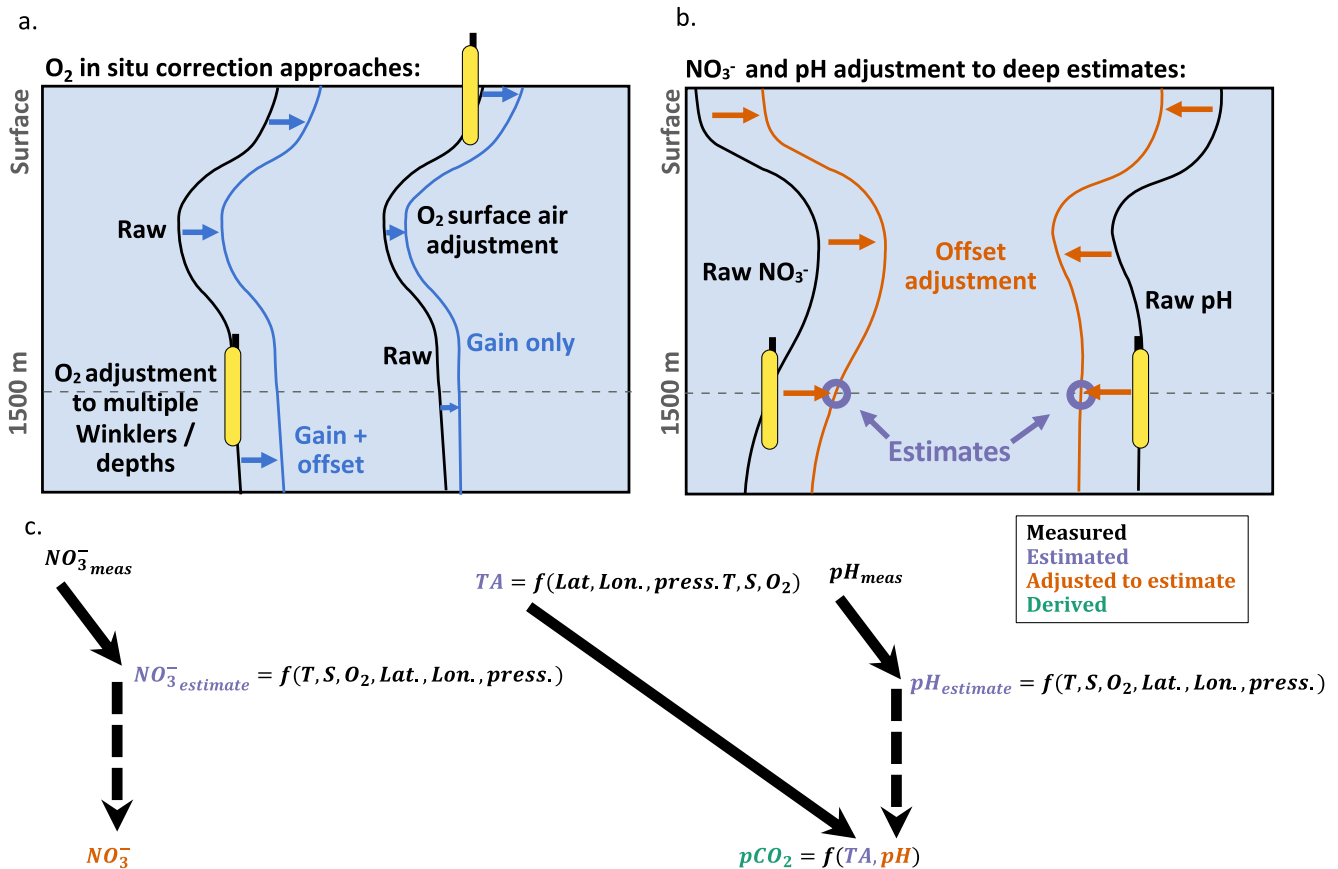
Figure 2. Schematic of the two primary in situ oxygen calibration approaches and how the calibrated oxygen data are used to adjust float pH and nitrate measurements. (a) Oxygen data collected on floats are typically calibrated using a gain and offset correction based on in situ data, typically collected at float deployment, or a gain-only correction based on air-calibration measurements made upon float surfacing throughout its lifetime. (b) Float nitrate and pH measurements are adjusted to algorithmic estimates of those parameters at 1,500 db in a way that impacts the whole profile. (c) Float measured T, S, oxygen, latitude, longitude, and pressure are input to the algorithms, which then predict the nitrate and pH at 1,500 db. The algorithms are either multiple linear regressions or neural networks trained on the GLODAP data set. Offsets between the float and ship oxygen will propagate through these algorithms into the adjusted nitrate and pH data.

where $p\mathrm{O}_2^{atmos}$ is the partial pressure of oxygen above the sea surface (atm), P_{Atm} is the local atmospheric pressure (atm), $p\mathrm{H}_2\mathrm{O}$ is the water vapor pressure at a given temperature and salinity (atm), RH is the relative humidity (%), and $\mathrm{X}_{\mathrm{O}_2}$ is the dry mole fraction of oxygen in the atmosphere (mol/mol) (Bushinsky et al., 2016). Float oxygen optodes are then calibrated either using an approach that tries to correct for splashing (Bittig & Körtzinger, 2015; Bittig, Körtzinger, et al., 2018) or using no splashing correction if the optode is high enough out of the water. The calibration also assumes that atmospheric water vapor pressure is at 100%. Evidence that optode drift at zero oxygen is minimal (Johnson et al., 2019; Maurer et al., 2021) has been used to justify a single multiplicative gain correction across the entire range of oxygen based on the difference between float air measurements and calculated atmospheric oxygen (Figure 2). This approach also assumes that the response of the oxygen optode at different oxygen levels and temperatures changes uniformly over time. Note that there is both a pressure effect on the optode response and on oxygen solubility that is added as an additional correction during optode processing.

The Global Ocean Data Analysis Project (GLODAP; Key et al., 2015; Olsen et al., 2016, 2020) is an ongoing international synthesis effort that evaluates surface-to-bottom ocean biogeochemical bottle data for outliers and internal consistency, which has been crucial to improving the accuracy and usability of shipboard data. In a similar effort, the Surface Ocean CO_2 Atlas (SOCAT) collects and assesses surface $p\mathrm{CO}_2$ measurements for accuracy prior to inclusion in an annual data product (Bakker et al., 2016). These efforts have been instrumental in our understanding of ocean biogeochemistry. There is currently no comparable, on-going, post-deployment census of float biogeochemical data to assess consistency within the float data set or between float and shipboard data. Most studies that have used Argo oxygen data and assessed their accuracy have focused on surface

data or analyzed changes measured by individual floats, thereby avoiding comparisons between different float measurements (Bushinsky & Emerson, 2015; Johnson et al., 2015; Martz et al., 2008; Wolf et al., 2018). As the float array expands and researchers begin using the entire data set as a whole or combining float and shipboard data sets to create global full-depth ocean oxygen products (e.g., World Ocean Atlas (WOA, Garcia et al., 2010); Gridded Ocean Biogeochemistry from Artificial Intelligence—Oxygen (Sharp et al., 2022)), attention must be paid to the accuracy of float oxygen data at depth.

Largescale comparisons of float and ship data sets indicate that, to a first order, float oxygen data have reached a comparable level of accuracy as ship-board measurements (Bushinsky et al., 2017; Johnson et al., 2017; Maurer et al., 2021). However, two float-to-ship comparisons of deep (1,500–2,000 m) oxygen data (Bushinsky et al., 2016; Drucker & Riser, 2016) indicate that surface calibration may not be a sufficient adjustment for the entire float oxygen profile. There is some indication that this could be due to inadequate calibration of the optode temperature response (Bittig, Körtzinger, et al., 2018), but Bushinsky et al. (2016) re-calibrated the optode temperature response for 11 floats in the lab prior to deployment, which did not address the difference in deep data; therefore, this approach does not seem to fully resolve the observed drift.

The accuracy of oxygen data throughout the water column is critical for understanding long-term changes in ocean oxygen content. At depth, the accuracy of quality-controlled float oxygen data is especially critical due to its use in adjusting other biogeochemical sensor data from Argo floats, which has downstream impacts on derived carbonate system parameters. Nitrate and pH sensors are now being deployed in large numbers (Claustre et al., 2020) and also require in situ adjustment to correct sensor drift (Maurer et al., 2021). Nitrate and pH measurements are adjusted using estimates of these parameters at 1,500 db that are derived from multiple linear regression or neural network algorithms trained on the GLODAP shipboard database (Bittig, Steinhoff, et al., 2018; Carter et al., 2016, 2021; Williams et al., 2016). These algorithmic estimates use inputs of temperature, salinity, depth, latitude, longitude, and, importantly, oxygen. Due to sensor response characteristics, adjustments to the nitrate and pH sensor data are applied almost uniformly to the entire profile; therefore, offsets at 1,500 m directly impact surface measurements (Maurer et al., 2021).

Float measurements of pH are widely used to estimate pCO_2 and other carbonate system parameters, using an algorithm-based estimate of total alkalinity (TA) and a carbonate system calculator. Many studies apply an additional adjustment to the quality controlled pH data prior to estimating pCO_2 that is meant to correct for an empirical pH-dependent pH bias (Carter et al., 2013, 2018; Williams et al., 2017). The accuracy of float pCO_2 estimates is critical as studies relying on float pCO_2 have identified significant differences between seasonal cycles of pCO_2, and wintertime air-sea CO_2 fluxes from studies that rely on shipboard pCO_2 alone (e.g., Bushinsky et al., 2019; Gray et al., 2018; Williams et al., 2016). Floats are measured year-round, including during winter months when rough weather makes shipboard observations rare, which provides immense observational value, if accurate. A number of studies have directly compared float pCO_2 estimates to shipboard observations (Bushinsky & Cerovečki, 2023; Coggins et al., 2023; Fay et al., 2018; Gray et al., 2018; Williams et al., 2017), while other studies have indirectly compared float pCO_2 and pH through assessment of other carbonate system parameters or CO_2 fluxes (e.g., Long et al., 2021; Mackay & Watson, 2021; Wu et al., 2022). A recent meta-analysis of float pCO_2 accuracy found biases are likely between 6 and 9 µatm (float pCO_2 high), with direct comparisons yielding lower biases (2–5 µatm) than indirect comparisons (Wu & Qi, 2023).

Here we use crossover comparisons between ship and float data to quantify differences in deep oxygen values and calculate the impact those offsets would have on adjusted and derived parameters. We refer to oxygen "offset", without strict attribution of the source of the error. Given the long-history and extensive use of Winkler titrations and the relatively short time-history of oxygen sensors and float-mounted oxygen sensors, we assume that the GLODAP values are likely correct and will present evidence later that supports this assumption.

2. Methods

2.1. Float and Shipboard Data Sets

Biogeochemical float data were downloaded on 22 October 2024 from the Argo Data Assembly Centers (DACs, closest snapshot: 09-10-2024 (Argo, 2023)) according to the list of floats with oxygen, nitrate, or pH sensors in the Argo Global DACs Synthetic-Profile Index file. 2,162 Argo floats deployed between 2002 and 2024 were included in this data set. Of these floats, 2,155 measured oxygen, of which 180,066 out of 308,994 profiles (58%)

contained valid delayed mode "ADJUSTED" oxygen data, meaning the data had been checked and/or corrected post deployment (median difference between uncorrected and adjusted data was 11 μmol kg^{-1}, adjusted data higher). 742 floats measured nitrate, with 54,795 profiles containing valid delayed mode adjusted data out of 85,701 total (64%). 653 floats measured pH, of which 27,326 profiles contained valid delayed mode adjusted data out of 61,851 total (44%). Only delayed mode and adjusted float data flagged as "good" and "probably good" (quality control flags 1 and 2, respectively) were used for this analysis. Float oxygen sensor calibration type for floats where crossovers with shipboard data were found was determined by reading the "SCIENTIFIC_CA-LIB_COMMENT" field (235 unique comments, Table S1 in Supporting Information S1) in float "Sprof" files and were categorized as: air, non-air, and bad/no calibration.

Shipboard bottle measurements of salinity, temperature, oxygen, nitrate, total CO_2 (DIC), or pH flagged as "good" from the GLODAP v2.2023 data set (Olsen et al., 2020) were used for comparison with float observations. The GLODAP data set was chosen because it includes a secondary quality control and adjustment to shipboard data for overall accuracy and internal consistency. Shipboard pH measurements in the GLODAP data set include a variety of measurement approaches. Carter et al., 2021, 2018 "homogenized" the GLODAP pH data set to be consistent with spectrophotometric pH measurements using purified meta-cresol purple (Liu et al., 2011) prior to training the LIPHR (Locally Interpolated PH Regression)/ESPER (Empirical Seawater Property Estimation Routine) algorithms. Algorithms such as LIPHR and ESPER use empirical relationships based on hydrographic cruise data to calculate a desired parameter based on commonly available measurements such as temperature, salinity, pressure, latitude/longitude, or oxygen. To recreate this homogenized data set, we used ESPER to calculate GLODAP pH (total pH scale) for every datapoint where a "good" pH measurement was present. By using the algorithms at the same datapoints on which they were trained, we recreated the homogenized data set and used this data for the pH crossover comparison. pH comparisons were made using pH values normalized to 25°C (pH$_{25-T}$) so that we removed the effect of any temperature differences in the carbonate system. DIC and TA are not changed by temperature and therefore do not need to be normalized.

2.2. Crossover Comparisons

Criteria for crossover comparisons between float and shipboard measurements were established using distance, pressure, potential density, and spice. For each float profile, we first found all GLODAP bottle measurements within a 100 km radius. Float data from 1,450 to 2,000 db were interpolated to a 1 db grid, with any gaps of over 125 db between successive float measurements removed from the interpolated profiles. Potential density (σ_θ) and spiciness (τ) relative to 0 db were calculated for both the float and shipboard data using the Gibbs SeaWater Oceanographic Toolbox of TEOS-10 for Python (McDougall & Barker, 2011). For each GLODAP bottle measurement between 1,400 and 2,100 db within the 100 km distance range, crossovers were determined by looking for interpolated float data with differences of less than ±0.005 kg m^{-3} σ_θ, ±0.005 τ, and ±100 db from the GLODAP sample properties. These difference thresholds were selected by analyzing levels of environmental oxygen noise in comparisons of individual floats against themselves using a range of density, spiciness, and distance thresholds (Text S1, Figure S1 in Supporting Information S1). Crossovers from any point in time were allowed. Mean property offsets (e.g., ΔC_{off}, for a given property "C") were calculated for floats with at least 20 oxygen crossovers and used in the results shown here (Figure S2 in Supporting Information S1 for float crossover examples). On average, offsets in the 1,450–2,000 db range did not differ significantly as a function of depth or concentration (Figure S3 in Supporting Information S1). While adjusting the filter criteria does impact the number of crossovers found for each float and can impact the mean offset calculated for an individual float, the overall results presented in this manuscript are relatively insensitive to the exact criteria used.

2.3. Impact of Oxygen Offsets on Derived Parameters

The impact of oxygen offsets (e.g., ΔC_{imp}, for a given property C) on float nitrate and pH adjustments and float estimated pCO_2 and DIC ($\Delta NO_3^-{}_{imp}$, $\Delta pH_{25-T,imp}$, $\Delta pCO_{2,imp}$, and ΔDIC_{imp}, respectively) was determined for each float with valid oxygen and nitrate or pH data and with a valid GLODAP crossover comparison. As previously described, oxygen offsets impact estimated pCO_2 and DIC through the effect of oxygen on the pH adjustment at 1,500 m (Figure 2). While oxygen is also used in the algorithmic estimation of total alkalinity, which is required for pCO_2 and DIC estimations, only a surface oxygen offset would impact the surface total alkalinity estimate, and subsequently the surface pCO_2 and DIC estimates, which are the foci of this work. Using temperature, salinity, and oxygen data at 1,500 m from each profile as inputs to the calibration algorithms, we

calculated pH and nitrate, both with and without adjusting for the mean float oxygen offset relative to GLODAP ($\Delta O_{2,off}$). We then calculated the differences in (impacts on) pH and nitrate with and without the $\Delta O_{2,off}$ correction ($\Delta pH_{25-T,imp}$ and $\Delta NO_3^-{}_{imp}$) and applied these differences to the adjusted full float profiles. This approach allows us to determine the impact a mean oxygen correction would have without attempting to replicate any step changes or non-linear adjustments that may have been applied during the original data adjustment procedure (Maurer et al., 2021). For nitrate, a uniform adjustment is applied to the entire nitrate profile. For pH, the adjustment at 1,500 m is scaled relative to the difference in temperature between each depth and 1,500 m, following the protocol used in the original pH measurement adjustment (Johnson et al., 2023). $\Delta pCO_{2,imp}$ and ΔDIC_{imp} were calculated using PyCO2SYS (v1.8.1; Humphreys et al., 2022, 2023) first with the original pH as an input and then with mean $\Delta pH_{25-T,imp}$ applied to the float profile and calculating the difference. Equilibrium constants of Dickson (1990), Lueker et al. (2000), and Perez and Fraga (1987) were used with PyCO2SYS and the Lee et al. (2010) boron to salinity ratio (Williams et al., 2017).

Floats equipped with pH and nitrate sensors have been deployed by many groups throughout the world. The majority have been deployed as part of SOCCOM or GO-BGC and adjusted by the data management teams of SOCCOM and the Monterey Bay Aquarium Research Institute (MBARI). Following adjustment approaches used by SOCCOM/MBARI, total alkalinity was calculated using LIARv2. ESPER could be used instead with largely similar results, but we opted to follow existing published approaches for ease of comparison. pH was calculated using ESPER (ESPER-mixed, an average of a neural network-based approach and an MLR; Carter et al., 2021) or LIPHR (Carter et al., 2018), and carbonate system calculations using PyCO2SYS. Both ESPER and LIPHR were used because SOCCOM pH data at the time of download have been adjusted to one of the two algorithms, depending on when the float was last active. Floats active prior to April 2023 were adjusted to LIPHR pH estimates, while floats active past this date were adjusted to ESPER pH. Figures and results shown in the main text rely on ESPER-based adjustments while the supplement includes results that rely on LIPHR-based adjustments, but average differences between the two are of a second order.

One complication is the presence of a pH-dependent pH correction (Williams et al., 2017) used by the SOCCOM/GO-BGC groups when calculating pCO_2. This correction accounts for the difference between float ISFET measured pH, which has been shown to align with spectrophotometric pH measurements (Takeshita et al., 2020), and pH values calculated from measurements of TA and DIC (Carter et al., 2013, 2018). It is currently unclear how to best apply a global correction similar to the one developed in Williams et al. (2017) and a recently published paper by a working group focused on inter-consistency in carbonate system measurements recommended removing this correction until a suitable correction for all float pH measurements can be developed (Carter et al., 2023). We have avoided dealing with this issue by looking at the difference between calculations with and without the oxygen offset impacts included. Any changes in this pH-dependent bias correction will represent a different additional impact to the float pCO_2 estimates. However, the impacts of the oxygen offset should be very similar for estimated pCO_2 with or without this additional pH-dependent bias correction.

3. Results

For floats where oxygen offsets could be determined, 93% of the offsets were statistically significant using a 1 sample *t*-test and a *p*-value threshold of 0.01 (Figures S2a and S2b in Supporting Information S1 for examples with significant and non-significant crossovers). Our goal is to quantify the potential impact of float oxygen offsets on other parameters, so we include all oxygen offset estimates, including non-significant ones, when calculating the mean oxygen offset and all floats with pH in the subsequent impact on derived parameters. Only including floats with a statistically significant oxygen offset would overstate the magnitude of the mean data set offset. However, if these crossover comparisons were used in the future to correct float oxygen data, it would be important to only adjust those floats with significant offsets so as not to over-adjust already good data.

The median oxygen offset for all floats is -1.9 μmol kg^{-1} (float minus GLODAP, $n = 660$) with a mean of -1.9 ± 3.9 (1 SD) μmol kg^{-1}, Figure 3a, Table S2 in Supporting Information S1) and a 95% confidence interval around the mean of -2.2 to -1.6 μmol kg^{-1}. Of the float oxygen sensors with valid crossovers, 305 had a non-air calibration method listed (median offset of -0.9 μmol kg^{-1}, mean of -1.0 ± 3.9, 95% CI $\{-1.4, -0.5\}$, μmol kg^{-1}), 307 were air calibrated (median offset of -2.7 μmol kg$^-$, mean of -3.0 ± 3.4 μmol kg^{-1}, 95% CI $\{-3.4, -2.7\}$), and 48 had bad calibration or no calibration listed, though they were still flagged as good data (median offset of -1.1 μmol kg^{-1}, mean of -1.3 ± 5.2 μmol kg^{-1}, 95% CI $\{-2.8, 0.2\}$) (Figure 3c). For floats
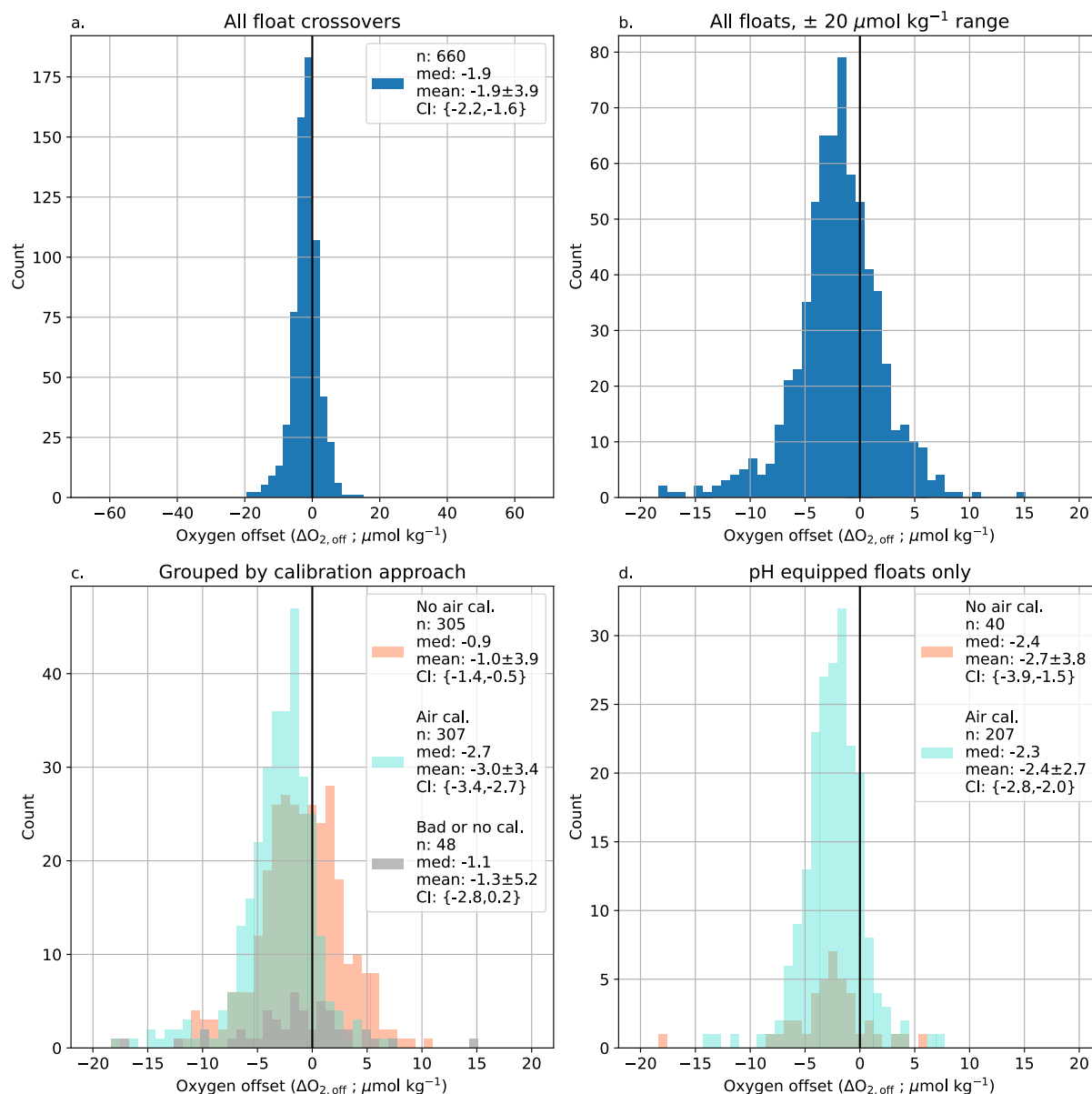
Figure 3. Histograms of float oxygen offsets relative to shipboard measurements. Float minus ship mean offsets between 1,450 and 2,000 db for all floats (a) with crossovers to GLODAP data and within ± 0.005 kg m^{-3} σ_θ, ± 0.005 τ, and ± 100 db. (b) Same as (a) but with a restricted x-axis range of ± 20 μmol kg^{-1}. (c) Offsets grouped by calibration type: non-air calibration listed (light red), air-calibrated (turquoise), and no calibration or bad calibration, though still marked as good data (orange). (d) Same as (c) but only showing data from non-air and air calibrated floats equipped with pH sensors. Figure legends list the number of floats, median offsets, mean offsets ± 1 SD, and 95% confidence intervals around the mean for each calibration category.

equipped with pH, non-air calibrated floats had a median oxygen offset of -2.4 μmol kg^{-1} ($n = 40$, mean of -2.7 ± 3.8 μmol kg^{-1}, 95% CI $\{-3.8, -1.5\}$) and air-calibrated floats had a median oxygen offset of -2.3 μmol kg^{-1} ($n = 207$, mean of -2.4 ± 2.7 μmol kg^{-1}, 95% CI $\{-2.8, -2.0\}$) (Figure 3d).

Offsets were also calculated between float and GLODAP measurements (with air-calibrated oxygen sensors) of nitrate and pH and between float estimates of DIC and GLODAP measurements (Figure 4, blue shaded histograms). The median difference between float and GLODAP nitrate measurements is 0.2 μmol kg^{-1} ($\Delta NO_3^-{}_{,off}$, $n = 264$, mean of 0.2 ± 0.4 μmol kg^{-1}, 95% CI $\{0.1, 0.2\}$). The median difference between float and GLODAP pH (normalized to 25°C, total pH scale) was -5.4 mpH (mpH = pH $\times$ 1,000; $\Delta pH_{25-T,off}$, $n = 106$, mean of -5.9 ± 7.7 mpH, 95% CI $\{-7.3, -4.4\}$). The median difference between DIC estimated from float pH and
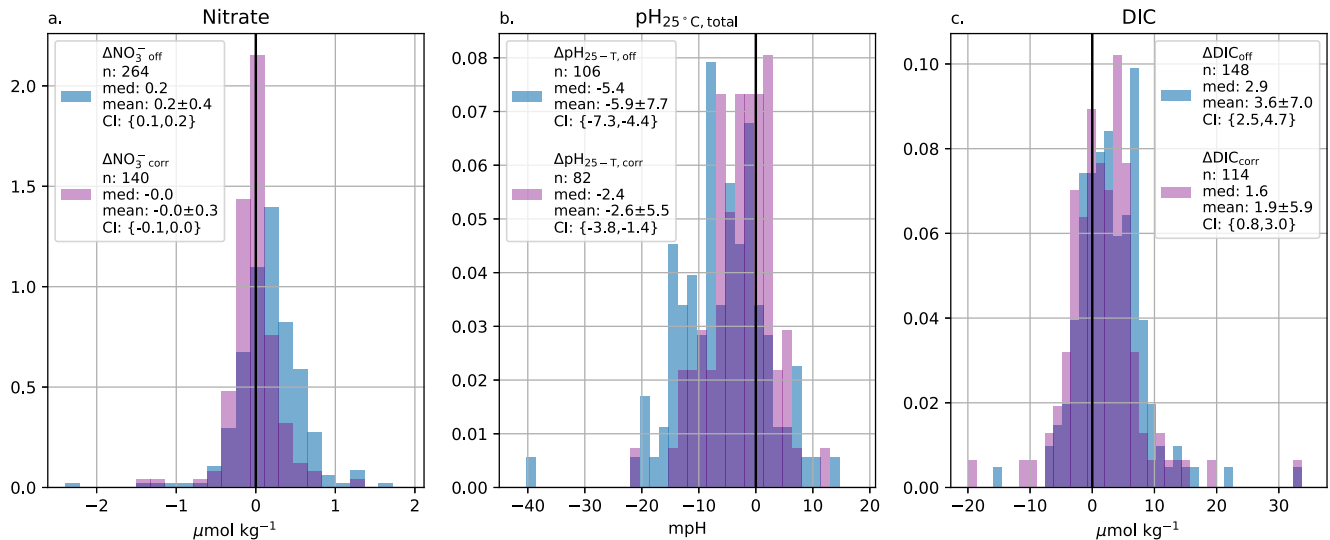
Figure 4. Frequency distributions of original nitrate (a), pH (b), and DIC (c) offsets relative to GLODAP crossovers ($\Delta NO_3^-{}_{,off}$, ΔpH_{off}, ΔDIC_{off}, blue shaded histograms) and crossover comparisons after the impact of correcting for the oxygen offset has been applied ($\Delta NO_3^-{}_{,corr}$, ΔpH_{corr}, ΔDIC_{corr}, purple shaded histograms). Correcting for the observed oxygen offset at depth fully corrects the nitrate offset relative to GLODAP and improves the median pH and DIC crossover comparisons by 3.0 mpH and -1.3 µmol kg^{-1}, respectively. Full statistics in Tables S3 and S4 of Supporting Information S1.

LIARv2 alkalinity and GLODAP DIC measurements is 2.9 µmol kg^{-1} (ΔDIC_{off}, $n = 148$, mean of 3.6 ± 7.0 µmol kg^{-1}, 95% CI {2.5, 4.7}, full statistics for nitrate, pH$_{25\text{-}T}$, and DIC crossovers in Table S3 of Supporting Information S1).

4. Discussion

4.1. Oxygen Offsets

The magnitude of the median offset is larger for air-calibrated floats (-2.7 µmol kg^{-1}) than non-air calibrated floats (-0.9 µmol kg^{-1}). This likely reflects that many non-air calibrated floats are corrected using both deep and near-surface shipboard values (e.g., to the WOA data set) or a full oxygen profile from a cast made at the deployment location (Figure 2) (Drucker & Riser, 2016; Takeshita et al., 2013), while air calibrated floats are primarily adjusted using a gain value derived from surface measurements of atmospheric oxygen over the float's lifetime (Bushinsky et al., 2016; Johnson et al., 2015, 2017; Maurer et al., 2021). The offsets shown in Figure 3 are small relative to the original correction from raw to "adjusted" oxygen (median difference between raw and adjusted float oxygen of -11 µmol kg^{-1}), but the mean offset for all comparisons other than the "Bad/no. cal" is significantly different from zero (95% confidence intervals, Figure 3 and Table S2 in Supporting Information S1) and, as we will discuss below, can have significant impacts on interpretation and use of this data.

The offset between float and shipboard data could reflect either that the float oxygen measurements are low or ship-based Winkler measurements are high. We will discuss both possibilities. It is important to recognize that we are considering approximately 12 different oxygen sensor models that utilize two different measurement principles made by three different manufacturers. The earliest oxygen sensors deployed on floats were initially Clark-cell electrodes (various SeaBird 43 models) while most current sensors are oxygen optodes made by multiple manufacturers but with the same basic sensing approach and chemistry (Figure 1). Here we primarily focus on possible offsets for oxygen optodes rather than Clark cell electrodes, and on air-calibrated optodes specifically, as these are the current state of the art sensors and represent the bulk of floats deployed with pH sensors.

If the offset between float and shipboard oxygen is due to low-biased float oxygen measurements, three possible causes of the offsets are: (a) an in situ difference in ocean oxygen content, (b) a residual uncorrected pressure response, or (c) a non-linear concentration-dependent drift in the sensor response. Basin-scale comparisons of float oxygen with shipboard measurements have indicated overall good float sensor accuracy in the surface ocean. A comparison of SOCCOM float oxygen data relative to GLODAP on pressure surfaces above and below the thermocline indicated that the air-calibrated float data at depth may be low by 2–3 µmol kg^{-1} (Bushinsky

et al., 2017). Johnson et al. (2017) assessed SOCCOM float data relative to float deployment cruises, across the full depth range, and against GLODAP crossovers within 20 km and below 300 m, finding that float oxygen was lower than shipboard measurements by 3.7 and 3.2 μmol kg^{-1} at "Midrange" (approximate water concentration of 250 μmol kg^{-1} [O$_2$]). Maurer et al. (2021) updated the Johnson et al. (2017) GLODAP comparison, finding a 3.6–3.8 μmol kg^{-1} low oxygen offset.

Although these earlier studies included shallower waters and compared data on pressure surfaces instead of using the combined σ$_θ$, τ, and pressure criteria of this study, all found similar magnitude and direction of differences. Maurer et al. (2021) attribute the mean [O$_2$] difference to a mean age difference of 18.6 years between the GLODAP and SOCCOM data sets due to the linear declines in Southern Ocean interior oxygen concentrations found in Helm et al. (2011). In Helm et al. (2011), the Southern Ocean has the largest region of oxygen change in the upper ocean (100–1,000 m) with the south Pacific and south Indian basins seeing changes of up to −0.7 μmol l^{-1} yr^{-1} between 1970 and 1992. However, deeper in the water column where we are conducting our crossover comparison (1,500–2,000 m), changes are of a smaller magnitude and appear to primarily be between 0 and −0.1 μmol l^{-1} yr^{-1} in the Southern Ocean and between −0.2 and + 0.2 μmol l^{-1} yr^{-1} across the global ocean. To rule out true oxygen changes as the source of offsets between the float and GLODAP data sets, we can assess the GLODAP data set for long-term oxygen changes and compare that oxygen change to the magnitude of float oxygen offsets.

If true oxygen changes at depth are responsible for the offsets found in our present study, we would expect the offset for a given float relative to GLODAP to be larger when compared to older cruise data and decrease in magnitude (typically becoming less negative) the closer in time between the float and GLODAP measurements. We therefore fit regressions to the float-GLODAP offsets as a function of time, calculating a 95% confidence interval around the regression, to determine if the regression ± CI included a zero offset at the midpoint time of the float deployment (see Figures S2a and S2b in Supporting Information S1 for examples of the regression and CI). 82 float offsets (12%) could be a result of observed change in oxygen concentration as determined by a trend in the GLODAP data set. However, in many of these cases there is simply too much uncertainty in the GLODAP oxygen regression with time or little to no difference between the float and shipboard data. While actual ocean oxygen change in the 1,450–2,000 db range remains a possible contributing factor to the differences seen between the float and shipboard oxygen levels, it does not seem to be the main cause.

The optode pressure correction combines a sensor pressure response with the pressure effect on oxygen solubility. Significant efforts have been made to determine the appropriate pressure correction between the optode response and oxygen partial pressure (e.g., Bittig et al., 2015; Uchida et al., 2008). We primarily focus on the mean oxygen offset for each float, averaging all crossover data from 1,450–2,000 db. However, if we bin the data by depth rather than pressure, we do not see a depth dependency in the float offsets in this depth range. While this may still exist, it does not seem to be a first order factor in the deep oxygen offset (Figure S3 in Supporting Information S1). A related issue is the lag in optode oxygen measurements due to the sensor response time (Bittig et al., 2014; Bittig & Körtzinger, 2017). Oxygen gradients at these depths are small, so is also not likely to be a first order issue but may contribute to the offset in some regions.

Optodes have been shown to not change response at zero oxygen (Johnson et al., 2015) and multiple calibrations over time have indicated relatively linear drift rates (Bittig & Körtzinger, 2015), lending support for the use of a gain correction across entire oxygen profiles. Bushinsky et al. (2016) measured greater drift rates at lower oxygen concentrations and postulated that the faster drift rate at low oxygen concentrations represents a deformation of the oxygen calibration surface, such that neither a gain nor an offset can be used to fully correct the range of oxygen measurements. Drucker and Riser (2016) show data from eight floats indicating that a near-surface gain correction leaves a negative offset at depth, similar to Bushinsky et al. (2016), but they did not provide an explanation. Both Bushinsky et al. (2016) and Drucker and Riser (2016) compared float data to bottle oxygen measurements from deployment casts, so oxygen change at depth did not play a factor. While we are still uncertain as to the mechanism causing low float oxygen values at depth relative to Winkler data, our current results from the entire oxygen Argo data set indicate that this does not seem to be an issue limited to a small number of floats and the possibility of non-linear drift in the oxygen calibration surface remains.

An alternative to the float oxygen measurement being biased low is that bottle measurements of oxygen using Winkler titrations are biased high due to contamination by atmospheric oxygen or impurities in reagents (Schmidtko et al., 2017). Sampling of oxygen and subsequent Winkler titration involves careful isolation of the

water from atmospheric contamination. Incomplete flushing or trapped bubbles can add a significant bias to Winkler data given that the low solubility of oxygen in water means that in equal volumes of air and water, the air will hold 50 times more oxygen than the water. GLODAP data has been QC'd and adjusted for internal consistency, but it is possible a bias is present in the deep data, especially if, on average, this bias is present in either all shipboard observations or the shipboard observations used as a reference for GLODAP adjustments.

Regardless of the source of the offset or mechanism for its existence, a systematic offset between float and shipboard oxygen measurements presents a problem for the current use of oxygen in float nitrate and pH parameter adjustment and derived parameter calculations. For all mechanisms other than a true change in ocean oxygen content, these offsets also complicate the determination of long-term ocean oxygen changes. Given the mean difference in float and GLODAP data set ages and that float oxygen measurements are now made in far greater numbers than shipboard data, a negative offset in the float data would appear in a combined data product as an increase in the true ocean oxygen loss signal. For the rest of this discussion, we focus on the impact of an oxygen offset on water properties derived from float measured data.
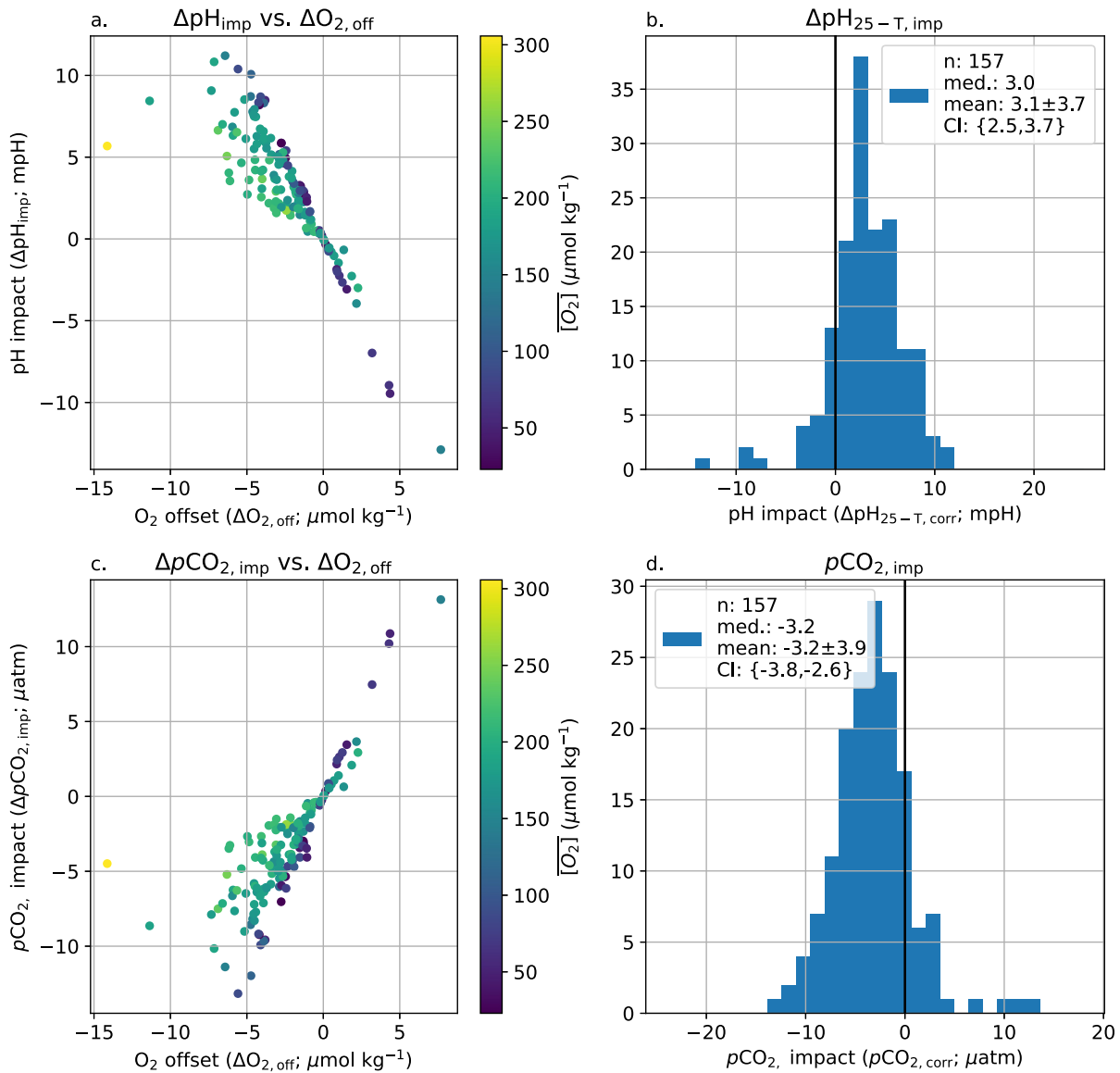
4.2. Impact of Oxygen Offsets on pH

As described earlier, float oxygen measurements at 1,500 m are used to correct for drift in the pH sensor data, which is then used with TA estimates to derive pCO_2 (Williams et al., 2017). We only consider here pH-equipped floats with air-calibrated oxygen, with equivalent figures and tables for all pH-equipped floats provided in the supplement. The median impact of correcting float pH for observed oxygen offsets was 3.0 mpH ($n = 157$, mean of 3.1 ± 3.7 mpH, 95% CI of 2.5–3.7 mpH, Figure 5, Table 1). The impact of oxygen offsets on pH corrections can be understood through the relationship between oxygen and inorganic carbon. A negative oxygen offset means that the float oxygen is lower than the expected value, so correcting the oxygen by a positive amount would result in a corresponding reduction in the apparent remineralization signature of the water mass. Higher oxygen and less remineralization would then imply lower dissolved inorganic carbon and therefore higher pH.

The sensitivity of the pH impact ($\Delta pH_{25-T,imp}$) to oxygen offset (represented as $\Delta pH_{25-T,imp}/\Delta O_{2,off}$) is between -0.4 and -2.3 mpH/(µmol kg^{-1}) (Figures 5 and 6). The largest $\Delta pH_{25-T,imp}$ values are observed in the Southern and Pacific Oceans, though the oxygen offsets do not show a similar spatial pattern. Instead, there is a spatial pattern to the $\Delta pH_{25-T,imp}/\Delta O_{2,off}$ that corresponds to the crossover oxygen concentration. The pH impact sensitivity (slope of the pH impact to O_2 offset) is greatest at low oxygen concentrations (Figures 5 and 6e), with the mean crossover oxygen concentration explaining 61% of the variance in calculated $\Delta pH_{25-T,imp}/\Delta O_2$ $_{Off}$ (Figure 6e).

This relationship can be understood by considering the changes in ocean chemistry as respiration takes place in a parcel of water. For example, we can take a parcel of water with initial TA and DIC of newly formed Subantarctic Mode Water from the southeast Pacific Ocean (Carter et al., 2014). If we then calculate the impact of organic matter respiration on oxygen, DIC, and TA, we can calculate the change in pH for every mole of oxygen respired. Initially, the $\Delta pH_{25-T,imp}/\Delta O_2$ $_{Off}$ is -2 mpH/(µmol kg^{-1}), but it drops to almost -2.8 mpH/(µmol kg^{-1}) after 250 µmol kg^{-1} of oxygen have been respired (Figure S10 in Supporting Information S1), as the buffer capacity of the water is eroded with increasing DIC; a situation that is analogous to surface ocean acidification. In the real ocean, regional differences in ocean interior biogeochemistry, including the buffer capacity, will cause regional differences in the sensitivity of pH to oxygen change. This likely accounts for a larger spread in the relationship between pH impact and oxygen offset for points in the Southern Ocean (Figure 6e), where there is significant mixing of different water masses.

4.3. Impact of Oxygen Offsets on Derived pCO_2

The median impact on float pCO_2 ($\Delta pCO_{2,imp}$) for correcting observed oxygen offsets is -3.2 µatm (air-calibrated floats only, -3.2 ± 3.9 µatm, 95% CI {$-3.8, -2.6$}, Figure 5, Table 1). A reduction of float derived pCO_2 by this magnitude would account for a large portion of the apparent bias in float pCO_2 described in Wu and Qi (2023). For many of the studies with direct crossover comparisons, an adjustment of -3.2 µatm would effectively eliminate the average observed differences between float and shipboard pCO_2. It should be noted that the range in impacts is much greater than the median (a range of pCO_2 impact between -13.2 and 13.1 µatm), with the impact on individual floats and regions differing from the median impact. Following pH, some of the greatest pCO_2 impacts are found in the Southern Ocean and Pacific (Figure 6). Similar results are found if LIPHR is used

Figure 5. 1,500 m pH and surface pCO_2 impact from associated oxygen offset. The calculated impact of correcting pH (top panels) and pCO_2 (bottom panels) for observed oxygen offsets. (a, c) are scatter plots of the change in pH and pCO_2 for a given oxygen offset, with the points colored by the mean oxygen concentration of the float crossover comparisons. Correcting a float oxygen sensor that is low of correct would increase the float pH and decrease derived pCO_2. (b, d) are histograms of the pH and pCO_2 impacts, with zero marked with a black line and mean ± 1SD, 95% confidence intervals around the mean, and median values listed in the figure legends. pH impacts shown are at 1,500 m, while pCO_2 impacts are from surface values. Results shown here are calculated using air-calibrated floats and the ESPER-mixed pH algorithm, equivalent results for LIPHR in Figure S4 of Supporting Information S1 and for all pH-equipped floats in Figures S5 and S6 of Supporting Information S1.

Table 1
Impact on pH at 1,500 db and Derived Surface pCO_2 of Observed Oxygen Offsets

	Count	Median	Mean ± 1 SD	p-value[a]	95.0% CI {low, high}	Min.	Max.
pH impact ($\Delta pH_{25-T,imp}$, mpH)[b]	157	3.0	3.1 ± 3.7	<0.001	{2.5, 3.7}	−12.9	11.2
pCO_2 impact ($\Delta pCO_{2,imp}$, μatm)	157	−3.2	−3.2 ± 3.9	<0.001	{−3.8, −2.6}	−13.2	13.1

[a]p-value testing the hypothesis that the mean impact is different from 0 at a 95% confidence level. [b]Impacts for pH calculated using ESPER-mixed. The impacts shown here are for air-calibrated floats only. Equivalent numbers for LIPHR in Table S5 of Supporting Information S1.
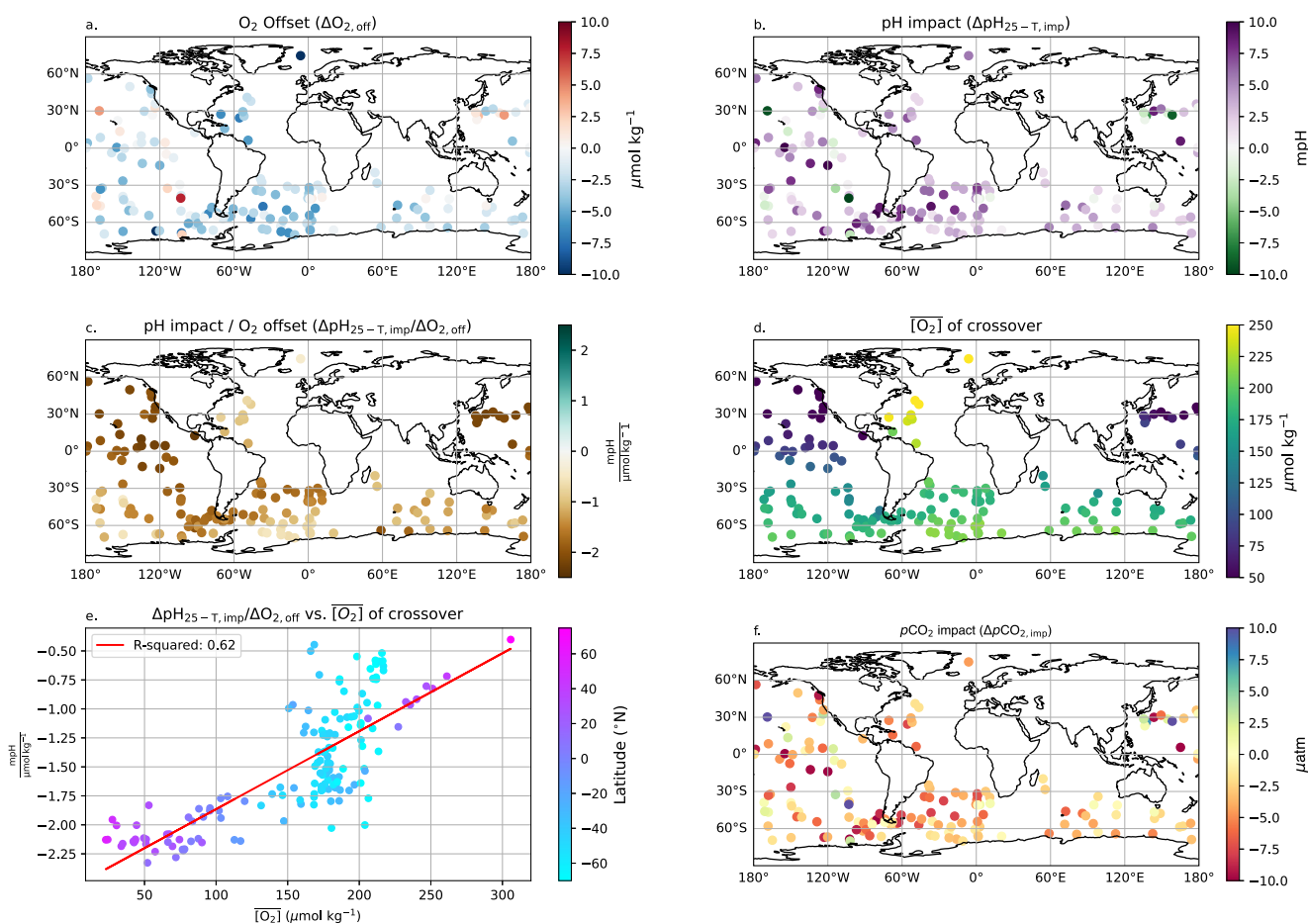
Figure 6. Relationships between oxygen offset, pH impact, mean oxygen concentration at crossover, and pCO_2 impact. Map of O_2 offset (a) demonstrates no obvious spatial pattern in the magnitude of offsets while the impact of correcting for the O_2 offsets on pH (b) tends to be greater in the Pacific and subpolar Southern Ocean. The ratio of the pH impact to O_2 offset ($\Delta pH_{25-T,imp}/\Delta O_{2,off}$, c) is greatest in the north Pacific and subpolar Southern Ocean, reflecting the mean oxygen concentration at crossover ($\overline{[O_2]}$, d). Plotting $\Delta pH_{25-T,imp}/O_{2,off}$ against $\overline{[O_2]}$ (e) and calculating a linear fit (red line) indicates that variations in $\overline{[O_2]}$ explain ~62% of the variance in $\Delta pH_{imp}/\Delta O_{2,off}$. Much of the deviation from the linear fit occurs in the Southern Ocean (light blue points). This response leads to stronger pCO_2 impacts (f) in the Pacific and subpolar Southern Ocean than in the North Atlantic or polar Southern Ocean. pH impacts shown are at 1,500 m, while pCO_2 impacts are from surface values. Results shown here are calculated using floats with air-calibrated oxygen and the ESPER-mixed pH algorithm, equivalent results for LIPHR in Figure S7 of Supporting Information S1 and for all pH-equipped floats in Figures S8 and S9 of Supporting Information S1.

to calculate pH impacts instead of ESPER, though with a slightly greater median and mean pCO_2 impact magnitude (median −3.4 μatm, mean of −3.8 ± 4.9, 95% CI {−4.5, −3.0} μatm, Table S5 in Supporting Information S1) and differences for individual floats.

To put a −3.2 μatm pCO_2 adjustment in context, Bushinsky et al. (2019) tested the impact of a 4 μatm systematic bias on calculations of Southern Ocean air-sea CO_2 fluxes using a mapped pCO_2 product based on both float pCO_2 estimates and the SOCAT pCO_2 data set. Adjusting float pCO_2 by −4 μatm changed the Southern Ocean CO_2 flux south of 35°S from −0.75 to −0.93 Pg C yr^{-1}. For comparison, their calculated Southern Ocean flux using shipboard data alone was −1.14 Pg C yr^{-1}. Therefore, a −3.2 μatm pCO_2 adjustment could have accounted for almost half of the difference between the Southern Ocean CO_2 flux calculated with and without float data. It is clear that systematic biases of this magnitude must be dealt with in order to increase the value of float pCO_2 estimates.

4.4. Impacts of Oxygen Offset on Nitrate and Derived DIC

As described above, relative to GLODAP float nitrate is offset high (0.2 μmol/kg), pH is offset low (−5.4 mpH), and DIC is offset high (2.9 μmol/kg, Table S3 in Supporting Information S1). These offsets are in approximately

the correct ratios and directions for a biological signal, either real or due to an offset in the oxygen measurement that is then propagated to pH and DIC. This indicates that the oxygen offset is most likely not due to a problem with the Winkler titrations.

The calculated impact on nitrate of the oxygen offset ($\Delta NO_3^-{}_{imp}$) is small (median of −0.2, mean of −0.2 ± 0.2, 95% CI {−0.2, −0.1} µmol kg^{-1}, Figure S11, Table S6 in Supporting Information S1), in keeping with Redfield stoichiometry of −16 N: 154 O$_2$ (Hedges et al., 2002) multiplied by an oxygen offset of ∼2 µmol kg^{-1}. The impact on DIC at 1,500 m of correcting for oxygen offsets is −1.0 µmol kg^{-1} (mean −1.1 ± 1.2 µmol kg^{-1} (CI {−1.3, −0.9}, Figures S12 and S13, Table S7 in Supporting Information S1), which is slightly smaller than multiplying the oxygen offset by a Redfield ratio of −106 C: 154 O$_2$.

As a check that the mean impacts ($\Delta NO_3^-{}_{imp}$, $\Delta pH_{25-T,imp}$) calculated from the oxygen offset would, in fact, improve the crossover comparisons with GLODAP data, we also re-ran the crossover comparison after applying the $\Delta O_{2,off}$, $\Delta NO_3^-{}_{imp}$ and $\Delta pH_{25-T,imp}$ to the original data. The resulting crossovers ($\Delta NO_3^-{}_{,corr}$, $\Delta pH_{25-T,corr}$, ΔDIC_{corr}, Figure 4, purple shaded histograms, statistics in Table S4 of Supporting Information S1) indicate that, on average, correcting the nitrate for the oxygen offset eliminates the entire nitrate offset, 3.0 mpH of the original −5.4 mpH pH offset, and 1.3 µmol kg^{-1} of the original 2.9 µmol kg^{-1} DIC offset.

The improvement in, but not full correction of, float-derived DIC and measured pH relative to the GLODAP crossovers provides an independent assessment that correcting the float data for this deep O$_2$ offset does, in fact, improve the pH data and subsequent carbonate system derived parameters. Furthermore, the fact that the nitrate bias appears to be fully corrected while the DIC, pH, and pCO$_2$ impacts only partially correct for the differences between float values and crossover or indirect comparisons gives an indication that the deep oxygen offset is not the only source of bias in the derived float carbonate parameters. This could be due to additional biases in the float pH, biases in the estimated TA, penetration of the ocean acidification signal to these depths, internal consistency issues with the marine carbonate system, or some other factors. It appears that correcting the oxygen may resolve a large fraction of the differences, but additional work remains to fully separate pCO$_2$, pH, and DIC biases in the float data from true signals.

Float oxygen crossovers with shipboard data are not available for all floats, making it difficult to determine the magnitude of an oxygen offset for all pH-equipped floats at this time. One option to reduce the possibility of an oxygen-induced bias in pH and derived pCO$_2$ is to correct float pH using an algorithm that does not use oxygen. Removing oxygen from the ESPER algorithm yields a 4.2 ± 6.0 mpH and −4.3 ± 6.4 µatm pCO$_2$ impact, somewhat larger than the 3.2 ± 3.8 mpH and −3.3 ± 4.1 µatm impact we calculated by applying the observed oxygen offset relative to GLODAP (Figure S14 in Supporting Information S1). Plotting the ESPER pH and pCO$_2$ impacts due to removing oxygen or correcting for the observed offset against one another yields a cluster of points around the 1:1 lines, though with considerable spread (Figure S15 in Supporting Information S1). This approach may indeed improve the derived parameters for floats with no GLODAP oxygen crossover for comparison, but is less accurate than if an oxygen correction is possible.

5. Conclusions

Here we identify an offset between float and ship-board oxygen measurements between 1,450 and 2,000 db. The magnitude of this offset is significant for studies assessing long-term ocean oxygen changes and for the use of float oxygen in adjusting pH and nitrate measurements and in subsequent calculated derived carbonate system quantities.

Correcting oxygen offsets of −2.3 µmol kg^{-1} in pH-equipped air-calibrated floats results in median pH impacts of 3.0 mpH and pCO$_2$ changes of −3.2 µatm. These differences are of similar direction and magnitude as many of the direct in situ comparisons between float pCO$_2$ estimates and underway pCO$_2$ measurements and therefore represent a first-order bias that needs to be addressed in the biogeochemical float data set. We do not definitively identify whether the oxygen offset is present in the float or ship-board data set, though the fact that correcting float oxygen would improve the nitrate, DIC, and pH crossover comparisons to shipboard data is a strong indication that the issue lies with the float observations.

Based on our findings, we offer the following recommendations:

1. The oxygen offsets described here represent an empirical correction that must be investigated to determine the underlying mechanism.
2. Float oxygen data at depth should be adjusted to historical shipboard data until our mechanistic understanding of the causes behind the float—ship differences is sufficient such that air calibration or other adjustments do not require a secondary correction.
3. Care should be taken in combining float and ship data, with an understanding that small biases may be present in either data set that could impact the usability of the data compilation to answer some scientific questions. The difference between the average age of the float and GLODAP data sets and the shift to float profile numbers greatly exceeding shipboard profiles in the 2000s means that any offset between the data sets will appear as a spurious change in ocean oxygen content. Additionally, individual floats may have significantly greater magnitude biases than the mean, and data should be assessed prior to any use relying on absolute accuracy.
4. Standardization of float sensor calibration comments and equations will make future studies of overall biogeochemical Argo float performance easier to perform.

Data Availability Statement

The "argo_synthetic-profile_index.txt" file used to determine biogeochemical Argo float WMO numbers and data locations was downloaded from ftp.ifremer.fr/ifremer/argo/dac. GLODAP data are available at https://glodap.info/index.php/merged-and-adjusted-data-product-v2-2022/. The analysis and plotting code used for this manuscript are available at https://doi.org/10.5281/zenodo.14722094 (Bushinsky et al., 2025).

References

Argo. (2000). *Argo float data and metadata from Global Data Assembly Centre (Argo GDAC)*. SEANOE. https://doi.org/10.17882/42182

Argo. (2023). Argo float data and metadata from Global Data Assembly Centre (Argo GDAC)—snapshot of Argo GDAC of June 09st 2023 [Dataset]. *SEANOE*. https://doi.org/10.17882/42182#103075

Bakker, D. C. E., Pfeil, B., Landa, C. S., Metzl, N., O'Brien, K. M., Olsen, A., et al. (2016). A multi-decade record of high-quality fCO_2 data in version 3 of the Surface Ocean CO_2 Atlas (SOCAT). *Earth System Science Data*, 8(2), 383–413. https://doi.org/10.5194/essd-8-383-2016

Bittig, H. C., Fiedler, B., Fietzek, P., & Körtzinger, A. (2015). Pressure response of Aanderaa and Sea-Bird oxygen Optodes. *Journal of Atmospheric and Oceanic Technology*, 32(12), 2305–2317. https://doi.org/10.1175/jtech-d-15-0108.1

Bittig, H. C., Fiedler, B., Scholz, R., Krahmann, G., & Körtzinger, A. (2014). Time response of oxygen Optodes on profiling platforms and its dependence on flow speed and temperature. *Limnology and Oceanography: Methods*, 12(8), 617–636. https://doi.org/10.4319/lom.2014.12.617

Bittig, H. C., & Körtzinger, A. (2015). Tackling oxygen optode drift: Near-surface and in-air oxygen optode measurements on a float provide an accurate in-situ reference. *Journal of Atmospheric and Oceanic Technology*, 32(8), 1536–1543. https://doi.org/10.1175/JTECH-D-14-00162.1

Bittig, H. C., & Körtzinger, A. (2017). Technical note: Update on response times, in-air measurements, and in situ drift for oxygen optodes on profiling platforms. *Ocean Science*, 13(1), 1–11. https://doi.org/10.5194/os-13-1-2017

Bittig, H. C., Körtzinger, A., Neill, C., van Ooijen, E., Plant, J. N., Hahn, J., et al. (2018a). Oxygen Optode sensors: Principle, characterization, calibration, and application in the Ocean. *Frontiers in Marine Science*, 4. https://doi.org/10.3389/fmars.2017.00429

Bittig, H. C., Steinhoff, T., Claustre, H., Fiedler, B., Williams, N. L., Sauzède, R., et al. (2018b). An alternative to static climatologies: Robust estimation of open ocean CO_2 variables and Nutrient concentrations from T, S, and O_2 data using Bayesian neural networks. *Frontiers in Marine Science*, 5(September), 328. https://doi.org/10.3389/fmars.2018.00328

Bushinsky, S. M., & Cerovečki, I. (2023). Subantarctic mode water biogeochemical formation properties and Interannual variability. *AGU Advances*, 4(2), e2022AV000722. https://doi.org/10.1029/2022AV000722

Bushinsky, S. M., & Emerson, S. (2015). Marine biological production from in situ oxygen measurements on a profiling float in the subarctic Pacific Ocean. *Global Biogeochemical Cycles*, 29(12), 2050–2060. https://doi.org/10.1002/2015GB005251

Bushinsky, S. M., Emerson, S. R., Riser, S. C., & Swift, D. D. (2016). Accurate oxygen measurements on modified Argo floats using in situ air calibrations. *Limnology and Oceanography: Methods*, 14(8), 491–505. https://doi.org/10.1002/lom3.10107

Bushinsky, S. M., Gray, A. R., Johnson, K. S., & Sarmiento, J. L. (2017). Oxygen in the Southern Ocean from Argo floats: Determination of processes driving air-sea fluxes. *Journal of Geophysical Research: Oceans*, 122(11), 8661–8682. https://doi.org/10.1002/2017JC012923

Bushinsky, S. M., Landschützer, P., Rödenbeck, C., Gray, A. R., Baker, D., Mazloff, M. R., et al. (2019). Reassessing Southern Ocean air-sea CO_2 flux estimates with the addition of biogeochemical float observations. *Global Biogeochemical Cycles*, 33(11), 1370–1388. https://doi.org/10.1029/2019GB006176

Bushinsky, S. M., Nachod, Z., Fassbender, A. J., Tamsitt, V., Takeshita, Y., & Williams, N. (2025). Offset between profiling float and shipboard oxygen observations at depth imparts bias on float pH and derived pCO2: Analysis and plotting code (Version R1_2025_01_22_v2). *Zenodo*. https://doi.org/10.5281/zenodo.14722094

Carpenter, J. H. (1965). The chesapeake Bay Institute technique for the Winkler dissolved oxygen method. *Limnology & Oceanography*, 10(1), 141–143. https://doi.org/10.4319/lo.1965.10.1.0141

Carter, B. R., Bittig, H. C., Fassbender, A. J., Sharp, J. D., Takeshita, Y., Xu, Y.-Y., et al. (2021). New and updated global empirical seawater property estimation routines. *Limnology and Oceanography: Methods*, 19(12), 785–809. https://doi.org/10.1002/lom3.10461

Carter, B. R., Feely, R. A., Williams, N. L., Dickson, A. G., Fong, M. B., & Takeshita, Y. (2018). Updated methods for global locally interpolated estimation of Alkalinity, pH, and Nitrate. *Limnology and Oceanography: Methods*, 16(2), 119–131. https://doi.org/10.1002/lom3.10232

Carter, B. R., Radich, J. A., Doyle, H. L., & Dickson, A. G. (2013). An automated system for spectrophotometric seawater pH measurements. *Limnology and Oceanography: Methods*, *11*(1), 16–27. https://doi.org/10.4319/lom.2013.11.16

Carter, B. R., Sharp, J. D., Dickson, A. G., Álvarez, M., Fong, M. B., García-Ibáñez, M. I., et al. (2023). Uncertainty sources for measurable ocean carbonate chemistry variables. *Limnology and Oceanography, lno*, *69*(1), 12477–12521. https://doi.org/10.1002/lno.12477

Carter, B. R., Talley, L. D., & Dickson, A. G. (2014). Mixing and remineralization in waters detrained from the surface into subantarctic mode water and Antarctic intermediate water in the Southeastern Pacific. *Journal of Geophysical Research: Oceans*, *119*(6), 4001–4028. https://doi.org/10.1002/2013JC009355

Carter, B. R., Williams, N. L., Gray, A. R., & Feely, R. A. (2016). Locally interpolated alkalinity regression for global Alkalinity estimation. *Limnology and Oceanography: Methods*, *14*(1998), 268–277. https://doi.org/10.1002/lom3.10087

Claustre, H., Johnson, K. S., & Takeshita, Y. (2020). Observing the Global Ocean with biogeochemical-Argo. *Annual Review of Marine Science*, *12*(1), 1–26. https://doi.org/10.1146/annurev-marine-010419-010956

Coggins, A., Watson, A. J., Schuster, U., Mackay, N., King, B., McDonagh, E., & Poulton, A. J. (2023). Surface ocean carbon budget in the 2017 South Georgia diatom bloom: Observations and validation of profiling biogeochemical Argo floats. *Deep Sea Research Part II: Topical Studies in Oceanography*, *209*, 105275. https://doi.org/10.1016/j.dsr2.2023.105275

D'Asaro, E. A., & McNeil, C. (2013). Calibration and stability of oxygen sensors on autonomous floats. *Journal of Atmospheric and Oceanic Technology*, *30*(8), 1896–1906. https://doi.org/10.1175/JTECH-D-12-00222.1

Dickson, A. G. (1990). Standard potential of the reaction: And the standard acidity constant of the ion HSO_4^- in synthetic sea water from 273.15 to 318.15 K. *The Journal of Chemical Thermodynamics*, *22*(2), 113–127. https://doi.org/10.1016/0021-9614(90)90074-Z

Dickson, A. G. (1994). Determination of dissolved oxygen in sea water by Winkler titration. *WHP Operations and Methods, (November)*, 1–13.

Drucker, R., & Riser, S. C. (2016). In situ phase-domain calibration of oxygen Optodes on profiling floats. *Methods in Oceanography*, *17*, 296–318. https://doi.org/10.1016/j.mio.2016.09.007

Emerson, S. (1987). Seasonal oxygen cycles and biological new production in surface waters of the subarctic Pacific Ocean. *Journal of Geophysical Research*, *92*(C6), 6535–6544. https://doi.org/10.1029/JC092iC06p06535

Fay, A. R., Lovenduski, N. S., Mckinley, G. A., Munro, D. R., Gray, A. R., Landschützer, P., et al. (2018). Utilizing the Drake passage time-series to understand variability and change in subpolar Southern Ocean pCO_2. *Biogeosciences Discussions*. https://doi.org/10.5194/bg-2017-489

Garcia, H. E., Locarnini, R. A., Boyer, T. P., Antonov, J. I., Baranova, O. K., Zweng, M. M., & Johnson, D. R. (2010). *World Ocean Atlas 2009 volume 3: Dissolved oxygen, apparent oxygen utilization, and oxygen saturation. Noaa Atlas Nesdic* (Vol. 70, p. 344). Government Printing Office. Retrieved from http://www.nodc.noaa.gov/OC5/indprod.html

Gray, A. R., Johnson, K. S., Bushinsky, S. M., Riser, S. C., Russell, J. L., Talley, L. D., et al. (2018). Autonomous biogeochemical floats detect significant carbon dioxide outgassing in the high-latitude Southern Ocean. *Geophysical Research Letters*, *45*(17), 9049–9057. https://doi.org/10.1029/2018GL078013

Gruber, N., Doney, S. C., Emerson, S. R., Gilbert, D., Kobayashi, T., Körtzinger, A., et al. (2009). *Adding oxygen to Argo: Developing a global in situ observatory for ocean deoxygenation and biogeochemistry*. Ocean Obs '09.

Gruber, N., Scott, C. D., Emerson, S. R., Gilbert, D., Kobayashi, T., Körtzinger, A., et al. (2007). The ARGO-oxygen program: A white paper to promote the addition of oxygen sensors to the international Argo float program.

Hedges, J. I., Baldock, J. A., Gélinas, Y., Lee, C., Peterson, M. L., & Wakeham, S. G. (2002). The biochemical and elemental compositions of marine plankton: A NMR perspective. *Marine Chemistry*, *78*(1), 47–63. https://doi.org/10.1016/S0304-4203(02)00009-9

Helm, K. P., Bindoff, N. L., & Church, J. A. (2011). Observed decreases in oxygen content of the global ocean. *Geophysical Research Letters*, *38*(23). https://doi.org/10.1029/2011GL049513

Hennon, T. D., Riser, S. C., & Mecking, S. (2016). Profiling float-based observations of net respiration beneath the mixed layer. *Global Biogeochemical Cycles*, *30*(6), 920–932. https://doi.org/10.1002/2016GB005380

Humphreys, M. P., Lewis, E. R., Sharp, J. D., & Pierrot, D. (2022). PyCO2SYS v1.8: Marine carbonate system calculations in Python. *Geoscientific Model Development*, *15*(1), 15–43. https://doi.org/10.5194/gmd-15-15-2022

Humphreys, M. P., Schiller, A. J., Sandborn, D., Gregor, L., Pierrot, D., van Heuven, S. M. A. C., et al. (2023). PyCO2SYS: Marine carbonate system calculations in Python (version v1.8.2). *Zenodo*. https://doi.org/10.5281/ZENODO.3744275

Johnson, K. S., Maurer, T. L., Plant, J. N., & Takeshita, Y. (2023). BGC-Argo quality control manual for pH [Pdf]. [object Object]. https://doi.org/10.13155/97828

Johnson, K. S., Plant, J. N., Coletti, L. J., Jannasch, H. W., Sakamoto, C. M., Riser, S. C., et al. (2017). Biogeochemical sensor performance in the SOCCOM profiling float array. *Journal of Geophysical Research: Oceans*, *122*(8), 6416–6436. https://doi.org/10.1002/2017JC012838

Johnson, K. S., Plant, J. N., Riser, S. C., & Gilbert, D. (2015). Air oxygen calibration of oxygen optodes on a profiling float array. *Journal of Atmospheric and Oceanic Technology*, *32*(11), 2160–2172. https://doi.org/10.1175/JTECH-D-15-0101.1

Johnson, K. S., Riser, S. C., & Ravichandran, M. (2019). Oxygen variability controls denitrification in the Bay of Bengal oxygen Minimum zone. *Geophysical Research Letters*, *46*(2), 1–8. https://doi.org/10.1029/2018GL079881

Key, R. M., Olsen, A., van Heuven, S., Lauvset, S. K., Velo, A., Lin, X., et al. (2015). Global Ocean Data Analysis Project, version 2 (GLODAPv2). *ORNL/CDIAC-162, NDP-093*. https://doi.org/10.3334/CDIAC/OTG.NDP093_GLODAPv2

Körtzinger, A., Schimanski, J., & Send, U. (2005). High quality oxygen measurements from profiling floats: A promising new technique. *Journal of Atmospheric and Oceanic Technology*, *22*(3), 302–308. https://doi.org/10.1175/JTECH1701.1

Lee, K., Kim, T.-W., Byrne, R. H., Millero, F. J., Feely, R. A., & Liu, Y.-M. (2010). The universal ratio of boron to Chlorinity for the North Pacific and North Atlantic oceans. *Geochimica et Cosmochimica Acta*, *74*(6), 1801–1811. https://doi.org/10.1016/j.gca.2009.12.027

Levin, L. A. (2018). Manifestation, drivers, and emergence of open ocean deoxygenation. *Annual Review of Marine Science*, *10*(1), 229–260. https://doi.org/10.1146/annurev-marine-121916-063359

Liu, X., Patsavas, M. C., & Byrne, R. H. (2011). Purification and characterization of meta-cresol purple for spectrophotometric seawater pH measurements. *Environmental Science & Technology*, *45*(11), 4862–4868. https://doi.org/10.1021/es200665d

Long, M. C., Stephens, B. B., McKain, K., Sweeney, C., Keeling, R. F., Kort, E. A., et al. (2021). Strong Southern Ocean carbon uptake evident in airborne observations. *Science*, *374*(6572), 1275–1280. https://doi.org/10.1126/science.abi4355

Lueker, T. J., Dickson, A. G., & Keeling, C. D. (2000). Ocean pCO_2 calculated from dissolved inorganic Carbon, Alkalinity, and equations for K1 and K2: Validation based on laboratory measurements of CO_2 in gas and seawater at equilibrium. *Marine Chemistry*, *70*(1–3), 105–119. https://doi.org/10.1016/S0304-4203(00)00022-0

Mackay, N., & Watson, A. (2021). Winter air-sea CO_2 fluxes constructed from summer observations of the Polar Southern Ocean suggest weak outgassing. *Journal of Geophysical Research: Oceans*, *126*(5). https://doi.org/10.1029/2020jc016600

Martz, T. R., Riser, S. C., & Johnson, K. S. (2008). Ocean metabolism observed with oxygen sensors on profiling floats in the South Pacific. *Limnology & Oceanography*, *53*(5), 2094–2111. https://doi.org/10.4319/lo.2008.53.5_part_2.2094

Maurer, T. L., Plant, J. N., & Johnson, K. S. (2021). Delayed-mode quality control of oxygen, Nitrate, and pH data on SOCCOM biogeochemical profiling floats. *Frontiers in Marine Science*, *8*(August), 1–20. https://doi.org/10.3389/fmars.2021.683207

McDougall, T. J., & Barker, P. M. (2011). *Getting started with TEOS-10 and the Gibbs Seawater (GSW) oceanographic Toolbox*. SCOR/IAPSO WG127. Retrieved from https://www.teos-10.org/pubs/Getting_Started.pdf

Olsen, A., Key, R. M., Van Heuven, S., Lauvset, S. K., Velo, A., Lin, X., et al. (2016). The Global Ocean Data Analysis Project version 2 (GLODAPv2)—an internally consistent data product for the world ocean. *Earth System Science Data*, *8*(2), 297–323. https://doi.org/10.5194/essd-8-297-2016

Olsen, A., Lange, N., Key, R. M., Tanhua, T., Bittig, H. C., Kozyr, A., et al. (2020). GLODAPv2.2020—The second update of GLODAPv2. *Earth System Science Data Discussions*. https://doi.org/10.5194/essd-2020-165

Perez, F. F., & Fraga, F. (1987). Association constant of fluoride and hydrogen ions in seawater. *Marine Chemistry*, *21*(2), 161–168. https://doi.org/10.1016/0304-4203(87)90036-3

Roemmich, D., Talley, L., Zilberman, N., Osborne, E., Johnson, K., Barbero, L., et al. (2021). The technological, scientific, and sociological revolution of global subsurface Ocean Observing. *Oceanography*, 2–8. https://doi.org/10.5670/oceanog.2021.supplement.02-02

Sarmiento, J. L., Johnson, K. S., Arteaga, L. A., Bushinsky, S. M., Cullen, H. M., Gray, A. R., et al. (2023). The Southern Ocean Carbon and Climate Observations and Modeling (SOCCOM) project: A review. *Progress in Oceanography*, *219*, 103130. https://doi.org/10.1016/j.pocean.2023.103130

Schmidtko, S., Stramma, L., & Visbeck, M. (2017). Decline in global oceanic oxygen content during the past five decades. *Nature*, *542*(7641), 335–339. https://doi.org/10.1038/nature21399

Schofield, O. A., Fassbender, A., Hood, M., Hill, K., & Johnson, K. (2022). A global ocean biogeochemical observatory becomes a reality. *Eos*, *103*. https://doi.org/10.1029/2022EO220149

Sharp, J. D., Fassbender, A. J., Carter, B. R., Johnson, G. C., Schultz, C., & Dunne, J. P. (2022). GOBAI-O$_2$: Temporally and spatially resolved fields of ocean interior dissolved oxygen over nearly two decades (preprint). *ESSD – Ocean/Chemical oceanography*. https://doi.org/10.5194/essd-2022-308

Stramma, L., & Schmidtko, S. (2021). Spatial and temporal variability of oceanic oxygen changes and underlying trends. *Atmosphere-Ocean*, *59*(2), 122–132. https://doi.org/10.1080/07055900.2021.1905601

Takeshita, Y., Johnson, K. S., Coletti, L. J., Jannasch, H. W., Walz, P. M., & Warren, J. K. (2020). Assessment of pH dependent errors in spectrophotometric pH measurements of seawater. *Marine Chemistry*, *223*, 103801. https://doi.org/10.1016/j.marchem.2020.103801

Takeshita, Y., Martz, T. R., Johnson, K. S., Plant, J. N., Gilbert, D., Riser, S. C., et al. (2013). A climatology-based quality control procedure for profiling float oxygen data. *Journal of Geophysical Research: Oceans*, *118*(10), 5640–5650. https://doi.org/10.1002/jgrc.20399

Tengberg, A., Hovdenes, J., Andersson, H. J., Brocandel, O., Diaz, R., Hebert, D., et al. (2006). Evaluation of a lifetime-based optode to measure oxygen in aquatic systems. *Limnology and Oceanography: Methods*, *4*(1964), 7–17. https://doi.org/10.4319/lom.2006.4.7

Uchida, H., Kawano, T., Kaneko, I., & Fukasawa, M. (2008). In situ calibration of optode-based oxygen sensors. *Journal of Atmospheric and Oceanic Technology*, *25*(12), 2271–2281. https://doi.org/10.1175/2008JTECHO549.1

Williams, N. L., Juranek, L. W., Feely, R. A., Johnson, K. S., Sarmiento, J. L., Talley, L. D., et al. (2017). Calculating surface ocean pCO$_2$ from biogeochemical Argo floats equipped with pH: An uncertainty analysis. *Global Biogeochemical Cycles*, *31*(3), 591–604. https://doi.org/10.1002/2016GB005541

Williams, N. L., Juranek, L. W., Johnson, K. S., Feely, R. A., Riser, S. C., Talley, L. D., et al. (2016). Empirical algorithms to estimate water column pH in the Southern Ocean. *Geophysical Research Letters*, *43*(7), 3415–3422. https://doi.org/10.1002/2016GL068539

Wolf, M. K., Hamme, R. C., Gilbert, D., Yashayaev, I., & Thierry, V. (2018). Oxygen saturation surrounding deep water formation events in the Labrador sea from Argo-O$_2$ data. *Global Biogeochemical Cycles*, *32*(4), 635–653. https://doi.org/10.1002/2017GB005829

Wu, Y., Bakker, D. C. E., Achterberg, E. P., Silva, A. N., Pickup, D. D., Li, X., et al. (2022). Integrated analysis of carbon dioxide and oxygen concentrations as a quality control of ocean float data. *Communications Earth & Environment*, *3*(1), 92. https://doi.org/10.1038/s43247-022-00421-w

Wu, Y., & Qi, D. (2023). The controversial Southern Ocean air-sea CO$_2$ flux in the era of autonomous ocean observations. *Science Bulletin*, *68*(21), 2519–2522. https://doi.org/10.1016/j.scib.2023.08.059

Yang, B., Emerson, S. R., & Bushinsky, S. M. (2017). Annual net community production in the subtropical Pacific Ocean from in situ oxygen measurements on profiling floats. *Global Biogeochemical Cycles*, *31*(4), 728–744. https://doi.org/10.1002/2016GB005545